Resilience-Driven Modeling, Operation and Assessment for a Hybrid AC/DC Microgrid

YI WANG[ID], (Student Member, IEEE), **ANASTASIOS OULIS ROUSIS**[ID], (Member, IEEE), **AND GORAN STRBAC**[ID], (Member, IEEE)

Department of Electrical and Electronic Engineering, Imperial College London, London SW7 2AZ, U.K.

Corresponding author: Yi Wang (yi.wang18@imperial.ac.uk)

ABSTRACT High-impact and low-probability extreme events can cause severe damage to power systems, especially for distribution systems. Microgrids (MGs) with distributed generation resources provide a viable solution for local load survivability via islanding schemes during extreme events. Recently, much research has focused on resilience-driven modeling and operations of MGs. In this paper, a resilience-driven operational model incorporating two operational modes (grid-connected and islanded) and detailed technical characteristics, such as voltage-related operational constraints, is developed for the resilience enhancement of a hybrid AC/DC MG. A detailed AC optimal power flow (OPF) algorithm is employed to model operational constraints and the power exchange between AC and DC subgrids. Preventive power importing is utilized for better preparedness before extreme events and demand response is employed to reduce load shedding during emergency mode. Existing literature on resilience assessment is reviewed and a modified multi-phase curve is proposed to fully represent the influence of limited generation resources and uncertain event duration on resilience. Extensive case studies capturing the distinction of critical loads and non-critical loads and two types of contingencies (multiple line faults and interrupted connection between AC subgrid and DC subgrid) are conducted to demonstrate the effectiveness of the proposed resilience strategy on protecting critical loads and reducing total load shedding. Particularly, a sensitivity analysis considering different event occurrence time has been simulated to capture, in a simple but rather effective way, the effect of the uncertainty surrounding event occurrence.

INDEX TERMS AC/DC hybrid microgrids, resilience, extreme events, AC optimal power flow, preventive power importing, demand response.

NOMENCLATURE
Abbreviations

MG	Microgrid
WT	Wind turbine
PV	Photovoltaic
DG	Distributed generators
BESS	Battery energy storage system
RI	Resilience index
OPF	Optimal power flow
EMS	Energy management system
AC	Alternating Current
DC	Direct Current

Parameters

β_f	The maximum percentage of shiftable loads for load type f
Δt	Time interval
δ^{lim}	Maximum permissible voltage angle variation between two buses
η_c	Efficiency of storage device(s) in bus b during charging
η_d	Efficiency of storage device(s) in bus b during discharging
γ_p	Interlinking converter active power droop gain
γ_q	Interlinking converter reactive power droop gain
ω_{max}	Maximum permissible value of frequency ω

ω_{min}	Minimum permissible value of frequency ω
B_{bp}	Susceptance of branch connecting AC buses b, p
G_{bp}	Conductance of branch connecting buses b, p
c_{buy}	Cost associated with power buying
c_{sell}	Cost associated with power selling
c_g	Cost associated with power generation
c_{ls}	Cost associated with load shedding
c_{os}	Cost associated with overslack (i.e. an artificial generator)
c_S^d	Cost associated with battery discharge
c_S^c	Cost associated with battery charge
T	Time scheduling horizon in preventive stage
T_e	Time scheduling horizon in emergency stage
T_f	Acceptable shifting time horizon of load type f
P_{ic}^{lim}	Power exchange limitation between AC and DC subgrids (active)
Q_{ic}^{lim}	Power exchange limitation between AC and DC subgrids (reactive)
Q_{gAC}^{max}	Maximum power of a generator g (reactive)
Q_{gAC}^{min}	Minimum stable generation of a generator g (reactive)
$\alpha_{AC(DC)}(b,t)$	Potential benefit associated with the storage level of bus b at time t in AC subgrid
$ES_{b_{AC(DC)}}^{max}$	Maximum state of charge
$ES_{b_{AC(DC)}}^{min}$	Maximum depth of discharge
$P_{g_{AC(DC)}}^{max}$	Maximum power of a generator g (active)
$P_{g_{AC(DC)}}^{min}$	Minimum stable generation of a generator g (active)
$P_{b_{AC(DC)}}^{max}$	Maximum storage power
$P_{b_{AC(DC)}}^{min}$	Minimum storage power
P_{Max}	Power exchange limitation between the main grid and the MG
$V_{AC(DC)}^{max}$	Maximum permissible AC(DC) voltage
$V_{AC(DC)}^{min}$	Minimum permissible AC(DC) voltage
$S_{AC(DC)}^{lim}(i)$	Capacity limit of branch i
$GS_{g_{AC(DC)}}^{ini}$	Initial state of generation resources in generator g during extreme events
$GS_{g_{AC(DC)}}^{min}$	Minimum energy reserve of generator g during extreme events

Sets

G_{bus}	Total number of generator buses, $G_{bus} \subset N_{bus}$
L_{bus}	Total number of load buses, $L_{bus} \subset N_{bus}$
N_{br}	Total number of branches
N_{bus}	Total number of buses
N_g	Total number of generators
S_{bus}	Total number of buses with storage device(s), $S_{bus} \subset N_{bus}$
$G_{bus_{AC(DC)}}$	Total number of AC(DC)-side generator buses
$L_{bus_{AC(DC)}}$	Total number of AC(DC)-side load buses
$N_{bus_{AC(DC)}}$	Total number of AC(DC)-side buses
$N_{g_{AC(DC)}}$	Total number of AC(DC)-side generators
$N_{L_{AC(DC)}}$	Total number of load types in AC(DC) side
$S_{bus_{AC(DC)}}$	Total number of buses with storage device(s) in AC(DC) side

Variables

Δe	Error between the normalized frequency, $\hat{\omega}$, and the normalized DC voltage, $\hat{V_{dc}}$
$\delta(b,t)$	Voltage angle of AC bus b at time t
$\delta_{bp}(t)$	Voltage angle difference between buses b, p at time t
$\hat{\omega}$	Normalized value of frequency ω
$\hat{V_{DC}}$	Normalized value of DC voltage
$P_{ic}(t)$	Active power flow through the interlinking converter at time t
$Q_{ic}(t)$	Reactive power flow through the interlinking converter at time t
$P_{buy}(t)$	Active power bought from the main grid at time t
$P_{SELL}(t)$	Active power sold to the main grid at time t
$ES_{AC(DC)}(b,t)$	Energy content in AC(DC) storage in bus b at the end of the current time step t
$GS_{AC(DC)}(g,t)$	Energy reserve of generator g in AC(DC) subgrid at the end of the current time step t
$P_{ex_{AC(DC)}}(b,t)$	Active power exchange between considered bus b and other buses at time t in the AC(DC) subgrid
$P_{OS_{AC(DC)}}(b,t)$	AC(DC) overslack for active power at bus b at time t
$P_{AC(DC)}(g,t)$	Active power generation of AC(DC) generator g at time t
$P_{l_{AC(DC)}}(b,t)$	Active AC(DC) load at bus b at time t
$P_{ls_{AC(DC)}}(b,t)$	Involuntary loss of active AC(DC) load at bus b at time t
$P_{lsh_{AC(DC)}}(b,f,t)$	Load shift of active AC(DC) load type f at bus b at time t
$Q_{AC}^{ex}(b,t)$	Reactive power exchange between considered bus b and other buses at time t
$Q_{AC}(g,t)$	Reactive power generation of AC generator g at time t

$Q_{l_{AC}}(b, t)$	Reactive AC(DC) load at bus b at time t
$Q_{ls_{AC}}(b, t)$	Involuntary loss of reactive AC load at bus b at time t
$Q_{os_{AC}}(b, t)$	AC overslack for reactive power at bus b at time t
$S_{AC(DC)}(i, t)$	Apparent power of AC(DC) branch i at time t
$P^c_{AC(DC)}(b, t)$	AC(DC) Storage charging into bus b at time t
$P^d_{AC(DC)}(b, t)$	AC(DC) Storage discharging from bus b at time t
$V_{AC(DC)}(b; t)$	Voltage at AC(DC) bus b at time t

I. INTRODUCTION

Extreme events, such as flooding and hurricanes, can cause severe damage to power systems. To deal with these (so-called) high-impact low-probability events, the concept of resilience has been introduced in power systems. Resilience refers to 'the ability of a system to anticipate and withstand external shocks, bounce back to its pre-shock state as quickly as possible and adapt to be better prepared to future catastrophic events' [1]. In [2], resilience is defined as a dynamic procedure for the improvement of robustness and operational flexibility against uncertainties. Given the large disruptions caused by extreme events, the primary aim for a resilient power system would be to provide power supply for critical loads (e.g. police stations, hospitals, and data centers). Recently, various studies have focused on the advantages of microgrids (MGs) on resilience enhancement. MGs with distributed generators (DGs), such as diesel generators, wind turbines (WTs) and photovoltaic (PVs), can restore local loads via islanding schemes or restore global loads via dynamic formation, if utility power supply is interrupted during extreme events. It can be anticipated that building-scale urban MGs will become common in the coming decades and play a crucial role in the development of future energy systems worldwide due to the essential benefits they provide for resilience enhancement in decentralized operating paradigms [3].

This paper mainly focuses on how to model and enhance the resilience of an AC/DC hybrid MG via effective islanding schemes. Existing research, challenges and our contributions on resilience-driven modeling, operation and assessment of MGs are summarized hereafter:

A. EXISTING RESEARCH ON RESILIENCE-DRIVEN MODELING AND OPERATIONS OF MGs

As far as the resilience-driven modeling and operations of MGs are concerned, various techniques have recently been proposed for the resilience enhancement of traditional AC MGs, since research in this area is a lot more mature. On the one hand, there is much research utilizing the grid-connected mode of AC MGs to make preparations for upcoming events via battery management or generator pre-scheduling. In [4], [5], a Benders decomposition method is suggested

to decompose a MG optimal modeling problem to normal operation and resilient operation problems respectively with the consideration of uncertain event time and duration. In [6], [7], resilience-driven MG operations based on vulnerability analysis are suggested to improve the preparedness of MGs against extreme events. However, these two papers do not consider the distinction of critical loads and non-critical loads. In [8], a risk-based energy management scheme is suggested to charge the battery energy storage systems (BESSs) in preventive stage for resilience enhancement. However, this paper only considers the operations of AC MGs in grid-connected mode. In [9], the size and operation of renewable energy (e.g. PV) with BESSs are optimized to minimize energy costs and increase the resilience of an AC MG. In [10], a resiliency function is proposed to allow an AC MG to operate under the islanded mode by importing power from nearby connected power systems and then have better preparedness against upcoming events. However, the above two papers assumes that the occurrence time of an extreme event can be accurately predicted, which can be unrealistic. On the other hand, there are also several papers only focusing on the resilience-driven modeling and operations of AC MGs in islanded mode. In [11], [12], proactive scheduling strategies based on vulnerability analysis, network reconfiguration and demand-side response are proposed to minimize load shedding. In [13], a preventive reinforcement strategy is suggested to identify the critical and vulnerable components in a multiple energy AC MG and increase the resilience against cyber-attacks. In [14], a defense resource planning and DG allocation problem against multi-period attacks is suggested to preserve the energy supply and mitigate the attack damage respectively. In [15], [16], corrective operations based on battery energy management and load shedding strategies are adopted to maximize economic performance or load survivability during extreme events. However, the outage duration is assumed to be known in [15], [16]. In [17], an event-triggered distributed control strategy is suggested to tackle the secondary restoration control of islanded AC MGs and reduce communication burden. Note that the above research on AC MGs (except for [15]) all assumes that there is unlimited energy supply during islanding period, which can be unrealistic in a resilience case.

In comparison with AC MGs, hybrid AC/DC MGs or DC MGs have the advantages to incorporate DC sources and loads, which is becoming more crucial because of the recent widespread of DC sources and loads [18]. In [19], future MGs are predicted to be hybrid AC/DC MGs. However, there is only limited research focusing on the development of resilience-driven operational strategies for AC/DC MGs or DC MGs. In [20]–[22], both feasible islanding and the survivability of critical loads are considered to enhances the resilience of a hybrid MG. Based on above research, a data-driven method is suggested in [23] to estimate the impact of dynamic uncertain bounds on the resilient operation of hybrid MGs and a demand response program is considered

to reduce load shedding during emergency period. In [24], a resilience-driven robust dispatching model is developed to obtain the robust plans in the worst scenario for a hybrid MG with the consideration of uncertain event occurrence time. In [25], a resilience analysis framework is put forward to study the fault ride-through capability of a DC MG against unknown cyber attacks. Note that these models on AC/DC hybrid MGs consider only power balance equations to control power flows. The omission of operational constraints relating to voltage, frequency and angle variation can lead to inaccurate solutions [26]. Additionally, except for [22], the rest of the papers all assume unlimited energy supply during islanded period.

B. EXISTING RESEARCH ON RESILIENCE ASSESSMENT

Maximizing load survivability or restoration is a widely-used objective in resilience-driven static modeling, while reducing frequency/voltage deviations is a commonly utilized objective in transient modeling approaches [27]. Much research has developed effective metrics to assess the resilience of the investigated systems and to satisfy the aforementioned objectives. Among these, a multi-phase resilience trapezoid model has been widely used to assess resilience strategies [1], [28], [29]. In [1], a multi-phase resilience assessment framework based on the $\Phi\Lambda E\Pi$ resilience metrics and an area metric is developed as well as both operational-oriented resilience and infrastructure-oriented resilience are evaluated via different metrics.

Based on this multi-phase curve, much research focusing on resilience-driven modeling has suggested corresponding assessment metrics. In [30], a preparedness index is developed to calculate the total storage of electrical and thermal before the event onset, which is used to assess the resilience of a distribution system in pre-disturbance phase. In [10], [23], a resilience index is proposed to assess the survivability of loads with different priorities. Similarly, a resilience metric is proposed in [31]–[33] to evaluate the contribution of a optimal strategy on critical load restoration during the restorative phase. In [34], three indices based on un-interrupted load and restored load are developed to capture the resistance, recovery and resilience of power systems. Unlike [2], [31], this paper both considers disturbance progress state and restorative state. Reference [35] presents a resilience index based on social welfare, which includes disturbance progress state, post disturbance state and restorative state. In [36], four indices, which include the average number of line trips, connectivity losses, load curtailments and a grid recovery index, are introduced to evaluate the resilience of power grids from both infrastructure view and operational view.

Note that the multi-phase resilience trapezoid model utilized in above research does not consider the influence of uncertain event duration and limited generation resources. It means the main features of extreme events are not accurately captured, which may lead to unrealistic decision making on planning and operations.

C. RESEARCH CHALLENGES

Overall, there are three research challenges discussed hereafter. The first challenge is how to capture the main features of extreme events and mimic a more realistic resilience scenario for case studies. Regarding the resilience-driven modeling of MGs, the above research (except for [15], [22]) all assumes that there is unlimited energy supply during islanding period, while many papers assume that the occurrence time and duration of extreme events can be predicted. Both of them can be unrealistic. References [15], [22] also fail to appropriately analyze the impact of limited generation resources on critical load shedding and total load shedding. Additionally, most existing literature tends to consider an islanding period shorter than 24 hours. However, a MG may stay in the islanded mode for a more extensive period of time, because of the difficulty to recover from extreme situations and reconnect to the grid [8]. It can be concluded that there is no significant research comprehensively considering main modeling details of a realistic resilience scenario, which shall definitely influence the accuracy and reality of optimal solutions.

The second challenge is how to develop a comprehensive operational strategy which can incorporate both preventive stage and corrective stage as well as the technical constraints relating to voltage, frequency and angle variation for the resilience enhancement of hybrid AC/DC MGs. Existing resilience-driven models on AC/DC hybrid MGs utilize energy management systems (EMSs) to model power flows, which can lead to inaccurate solutions. To the best of the authors' knowledge, there is no significant research focused on resilience-driven operation of AC/DC MGs with the consideration of operational constraints. Additionally, flexible technologies, such as BESSs and demand side response, will be progressively found in all types of energy systems in the future, especially in MGs. The existence of storage units and other flexible technologies can make MGs more robust and with stronger abilities to deal with contingencies caused by extreme events. As far as demand-side response is concerned, the impact of the percentage of shiftable loads on resilience enhancement of hybrid MGs (e.g. reducing load shedding and operational cost) has not been appropriately studied in existing literature.

The third challenge is how to suggest a more appropriate resilience curve to assess the resilience of hybrid AC/DC MGs. Optimization based on the multi-phase curve suggested by [2] includes two assumptions: i) unlimited energy supply (e.g. unlimited fuels, abundance of solar irradiation, wind, etc. during the event); ii) perfectly predicted outage occurrence time and duration, which ensure the continuity between post-restorative state and infrastructure recovery state. However, extreme events can disrupt energy supply chains, such as gas networks and fuel networks, which may result in the limitation of generation resources. Outage duration can not be accurately predicted because of the highly uncertain nature of extreme events. If MGs are used to supply loads over a specific period, they may fail to operate and the performance

curve (e.g. restored load) will drop again. Additionally, subsequent damage from extended events may cause further performance degradation. Under above situations, the multi-phase curve proposed in [2] may not accurately describe the operational state of networks.

D. CONTRIBUTIONS

Our first contribution is to consider an as realistic as possible resilience-based scenario for accurate optimal solutions. Within this context, limitation of generation resources, uncertain event occurrence time and two types of contingencies, including multiple line faults and the interrupted connection between two subgrids, are investigated capturing main features of extreme events (high uncertainty and severity) and further verifying the effectiveness of the proposed operational strategy. The distinction of critical loads and non-critical loads is also considered. Additionally, to clearly show the influence of limited generation resources, we investigate an islanding period lasting 48 hours after extreme events.

Our second contribution is to develop an effective and comprehensive operational strategy incorporating both grid-connected mode and islanded mode for the resilience enhancement of an AC/DC hybrid MG. In grid-connected mode, the objective is to minimize the operational cost and to import power from the main grid to be prepared for upcoming events, while the primary objective in islanded mode is to maximize load survivability. Day-ahead scheduling is used to appropriately demonstrate the benefits of BESSs and demand shifting on resilience enhancement. A detailed AC OPF algorithm suggested by [26] is incorporated into the proposed model instead of a simple energy management strategy in order to yield more accurate solutions capturing critical operating characteristics, such as voltage profiles.

Our third contribution is to suggest a modified multi-phase curve to show the influence of limited generation resources and uncertain event time and duration on optimal results. Based on the multi-phase curve, an area index is proposed to assess resilience and the influence of contingencies. The accuracy of this modified curve is verified via appropriate case studies.

The paper is organized as follows: Section II suggests a modified multi-phase curve based on limited generation resources and unknown event duration to capture the uncertain nature of extreme events. Section III introduces the model formulation in grid-connected mode and island mode and suggests a resilience strategy based on preventive power importing and demand shifting to reduce load shedding and particularly maximize critical load survivability, followed by extensive case studies in Section IV. Finally, in Sections V and VI, discussion provides insights on the analysis and subsequently conclusions are drawn.

II. A MODIFIED MULTI-PHASE RESILIENCE CURVE
In this paper, a modified multi-phase resilience curve is proposed in Fig. 1 to describe a more realistic operational state of MGs against extreme events. This curve considers
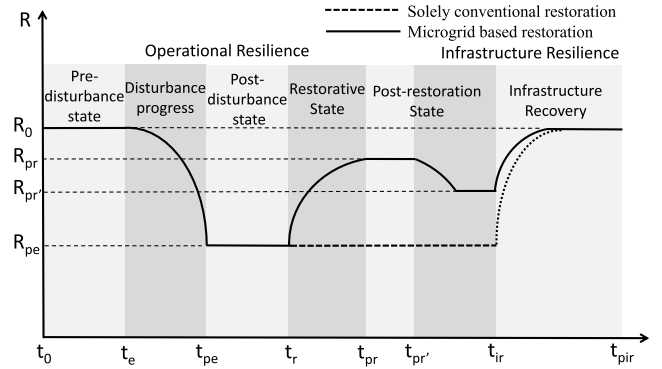

FIGURE 1. The modified multi-phase resilience curve.

the influence of limited generation resources and uncertain outage duration. According to this curve, the performance of a MG (e.g. restored load) will drop when the outage duration is longer than MG runtime and the MG does not have enough energy reserve to supply loads. In Fig. 1, pre-disturbance state, disturbance progress and post-disturbance state from t_0 to t_r are same as the corresponding states in the curve suggested by [2]. MGs are used to improve system performance from t_r to t_{ir}. The performance $R(t)$ drops again from $t_{pr'}$ to t_{ir} because of limited generation resources. For instance, there are several islanded MGs dynamically formulated and each MG has different limited energy reserve. On the one hand, the MG with minimal energy capacity firstly fails to operate and the performance curve drops, while other MGs can operate normally. Performance index $R_{pr'}$ may be equal to R_{pe}, if all the MGs fail to operate before the utility power supply is restored. On the other hand, the performance curve will be same as that in [2] ($R_{pr'} = R_{pr}$), if the utility repair time is shorter than the runtime of every MG during a given extreme event.

Based on this new multi-phase curve, a resilience index (RI) (1) is used to evaluate the effects of MGs on load survivability, which corresponds to the percentage of total curtailed loads before infrastructure restoration starts (e.g. dispatch of repair crews). This area metric will be 0 when a MG can entirely restore all the loads within this period, while a bigger RI is coupled with worse performance of MGs. Note that, in this paper, the original performance R_0 (i.e. pre-disturbance state) and the real-time performance $R(t)$ (i.e. performance across the event evolution) consider both critical loads and non-critical loads. As such, $R(t)$ can be calculated by the performance of critical loads $R_c(t)$ and non-critical loads $R_n(t)$, which are multiplied by different weighting factors w_c and w_n respectively. Note that selection of the weighting factors w_c and w_n indicates the significance of critical loads and non-critical loads ($w_c > w_n$).

$$RI = \frac{\int_{t_r}^{t_{ir}}(R_0 - R(t))}{R_0(t_{ir} - t_r)},$$
$$where\ R_0 = w_c R_c + w_n R_n,$$
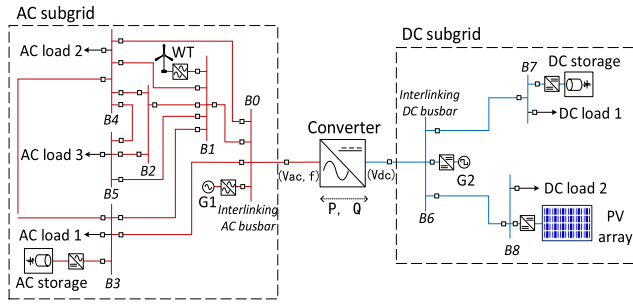$$R(t) = w_c R_c(t) + w_n R_n(t). \quad (1)$$

FIGURE 2. Schematic of the hybrid AC/DC MG under consideration.

III. PROBLEM FORMULATION

The topology of the utilized hybrid AC/DC MG is presented in Fig. 2. AC and DC subgrids are linked through an interlinking converter. Both AC subgrid and DC subgrid have a conventional generator (e.g. diesel generators in AC side and fuel cells in DC side) and a battery energy storage system (BESS). In the AC subgrid, a wind turbine (WT) is installed as renewable energy resource, while a PV is used as renewable energy resource in the DC subgrid.

A. RESILIENCE OPERATION MODE

Before receiving the first alert signal, the objective is to minimize operational cost, while the main goal after the alert is to try to keep a high level of energy stored in BESS units as well as to reduce operational cost, which is given in (2). The operational cost includes the cost from power exchange with main grid, generation cost and load shedding cost. The first six terms refer to generation cost, load shedding cost and overslack cost in AC and DC subgrids respectively. Overslack cost is included to avoid infeasibilities, and in practice it is modeled as an artificial and expensive generator. The following four terms correspond to the cost relating the charging/discharging behaviors of BESSs in AC and DC subgrids. The next term is the cost of power exchange with main grid, while the last two terms relate to the energy storage level of BESS units in AC and DC subgrids respectively. Because the occurrence time and duration of extreme events cannot be accurately predicted, the MG will start being prepared after receiving the first warning. In other words, the MG will try to keep a high energy storage level of BESS units in the whole preventive stage. Therefore, the values of coefficients α_{AC} and α_{DC} shall be larger than the generation and power exchange cost. Note that this formulation is rather generic and complete to ensure that all cases are captured; nevertheless, certain equations/parameters (e.g. the buying/selling price of the BESSs) are not applicable to the presented case studies.

$$
\begin{aligned}
F_1 &= \sum_{t\in T}\sum_{g\in N_{g_{AC}}} c_g P_{AC}(g,t) + \sum_{t\in T}\sum_{b\in L_{bus_{AC}}} c_{ls}P_{ls_{AC}}(b,t) \\
&+ \sum_{t\in T}\sum_{g\in N_{g_{DC}}} c_g P_{DC}(g,t) + \sum_{t\in T}\sum_{b\in L_{bus_{AC}}} c_{ls}P_{ls_{DC}}(b,t)
\end{aligned}
$$

$$
\begin{aligned}
&+ \sum_{t\in T}\sum_{b\in L_{bus_{AC}}} c_{os}P_{os_{AC}}(b,t) + \sum_{t\in T}\sum_{b\in L_{bus_{DC}}} c_{os}P_{os_{DC}}(b,t) \\
&+ \sum_{t\in T}\sum_{b\in S_{bus_{AC}}} c_S^d P_{AC}^d(b,t)\eta_d - \sum_{t\in T}\sum_{b\in S_{bus_{AC}}} c_S^c P_{AC}^c(b,t)\eta_c \\
&+ \sum_{t\in T}\sum_{b\in S_{bus_{DC}}} c_S^d P_{DC}^d(b,t)\eta_d - \sum_{t\in T}\sum_{b\in S_{bus_{DC}}} c_S^c P_{DC}^c(b,t)\eta_c \\
&+ \sum_{t\in T} c_{buy}P_{buy}(t) - \sum_{t\in T} c_{sell}P_{sell}(t)) \\
&- \sum_{t\in T}\sum_{b\in S_{bus_{AC}}} \alpha_{AC} ES_{AC}(b,t) \\
&- \sum_{t\in T}\sum_{b\in S_{bus_{DC}}} \alpha_{DC} ES_{DC}(b,t)
\end{aligned}
\tag{2}
$$

The optimization problem is posed as a minimization problem, subject to the constraints represented by (3)-(23). Active and reactive power balance equations at each bus b are shown in (3) and (4) and the classical equations pertaining to power flow problems are presented in (5) and (6). Equation (7) shows the power buying and power selling cannot occur simultaneously and equation (8) corresponds to the power exchange limit between the MG and main grid.

$$
\begin{aligned}
P_{buy}(t) - P_{sell}(t) &+ P_{AC}^d(b,t) - P_{AC}^c(b,t) \\
&+ \sum_{g\in NG_b} P_{AC}(g,t) + P_{ls_{AC}}(b,t) \\
&= P_{AC}^{ex}(b,t) + P_{l_{AC}}(b,t) \\
&+ P_{os_{AC}}(b,t) + P_{ic}(t)
\end{aligned}
\tag{3}
$$

$$
\begin{aligned}
\sum_{g\in NG_b} Q_{AC}(g,t) &+ Q_{ls_{AC}}(b,t) \\
&= Q_{AC}^{ex}(b,t) + Q_{l_{AC}}(b,t) \\
&+ Q_{os_{AC}}(b,t) + Q_{ic}(t)
\end{aligned}
\tag{4}
$$

$$
\begin{aligned}
P_{AC}^{ex}(b,t) = \sum_{p\in N_{bus_{AC}}} &V_{AC}(b,t)V_{AC}(p,t) \\
(G_{bp}\cos\delta_{bp}(t) + B_{bp}\sin\delta_{bp}(t)), \quad \forall t\in T, \ \forall b\in N_{bus_{AC}}
\end{aligned}
\tag{5}
$$

$$
\begin{aligned}
Q_{AC}^{ex}(b,t) = \sum_{p\in N_{bus_{AC}}} &V_{AC}(b,t), V_{AC}(p,t) \\
(G_{bp}\sin\delta_{bp}(t) - B_{bp}\cos\delta_{bp}(t)), \quad \forall t\in T, \ \forall b\in N_{bus_{AC}}
\end{aligned}
\tag{6}
$$

$$
P_{buy}(t) \cdot P_{sell}(t) = 0, \quad \forall t\in T \tag{7}
$$

$$
P_{buy}(t), P_{sell}(t) \le P_{Max}, \quad \forall t\in T \tag{8}
$$

Note that $P_{ic}(t)$ and $Q_{ic}(t)$ in (3) and (4) represent the power flow through the interlinking converter connecting AC and DC grids. They are determined by (9) based on a droop control strategy, while power exchange limits can be found in (10). Δe represents the difference between the frequency and DC voltage, which can be found in (11). A normalization procedure called 'feature scaling' in statistics is utilized to bring the measurements in a per unit basis, as described by (12) and (13). Therefore, the given dataset in values are

converted within the range of [-1,1] to allow comparison of $\hat{\omega}$ and $\hat{V}_{DC}$ and then calculate Δe. This procedure effectively couples DC voltage and AC frequency and eventually obtains the resulting power sharing. More details about the implemented droop control strategy can be found in [26], [37]. Additionally, the control strategy utilized in the paper mainly considers two AC and DC subgrids with matched capacities. Power management strategies on multiple subgrids with different capacities can be found in [38], [39].

$$P_{ic} = -\frac{1}{\gamma_p}\Delta e, \quad Q_{ic} = -\frac{1}{\gamma_q}\Delta e \quad (9)$$

$$|P_{ic}| \le P_{ic}^{lim}, \quad |Q_{ic}| \le Q_{ic}^{lim} \quad (10)$$

$$\Delta e = \hat{\omega} - \hat{V}_{DC} \quad (11)$$

$$\hat{\omega} = \frac{2 \cdot \omega - (\omega_{max} + \omega_{min})}{\omega_{max} - \omega_{min}} \quad (12)$$

$$\hat{V}_{DC} = \frac{2 \cdot V_{DC} - (V_{DC}^{max} + V_{DC}^{min})}{V_{DC}^{max} - V_{DC}^{min}} \quad (13)$$

Equations (14)-(16) represent the operational constraints regarding voltage limits, line capacities and angle variation, while equations (17)-(18) correspond to the power generation limit of conventional generators. Given that a detailed AC OPF is employed to model a hybrid MG capturing voltage and frequency, ramp-up and ramp-down constraints have not been considered as no significant changes of generation would be allowed within one time interval. Inequalities (19) and (20) denote the limits for the charging and discharging power of BESSs, while equation (21) ensures that charging and discharging cannot occur simultaneously. Equation (22) gives the limits for minimum and maximum energy storage, which can also be presented via the state-of-charge (SOC) level. The dependence of energy storage level at each time interval on the previous time step is introduced in equation (23).

$$V_{AC}^{min} \le V_{AC}(b,t) \le V_{AC}^{max}, \quad \forall t \in T,$$
$$\forall b \in N_{bus_{AC}} \quad (14)$$

$$max(S_{AC}(i,t)) \le S_{AC}^{lim}(i), \quad \forall t \in T,$$
$$\forall i \in N_{br_{AC}} \quad (15)$$

$$|\delta(b,t) - \delta(p,t)| \le \delta_{AC}^{lim}, \quad \forall t \in T,$$
$$\forall b, p \in N_{bus_{AC}} \quad (16)$$

$$P_{g_{AC}}^{min} \le P_{AC}(g,t) \le P_{g_{AC}}^{max},$$
$$\forall t \in T, \ \forall g \in N_{g_{AC}} \quad (17)$$

$$Q_{g_{AC}}^{min} \le Q_{AC}(g,t) \le Q_{g_{AC}}^{max},$$
$$\forall t \in T, \ \forall g \in N_{g_{AC}} \quad (18)$$

$$0 \le P_{AC}^c(b,t) \le P_{b_{AC}}^{max},$$
$$\forall t \in T, \ \forall b \in S_{bus_{AC}} \quad (19)$$

$$0 \le P_{AC}^d(b,t) \le P_{b_{AC}}^{max},$$
$$\forall t \in T, \ \forall b \in S_{bus_{AC}} \quad (20)$$

$$P_{AC}^c(b,t) \cdot P_{AC}^d(b,t) = 0, \quad \forall t \in T, \ \forall b \in S_{bus_{AC}} \quad (21)$$

$$ES_{b_{AC}}^{min} \le ES_{AC}(b,t) \le ES_{b_{AC}}^{max},$$
$$\forall t \in T, \ \forall b \in S_{bus_{AC}} \quad (22)$$

$$ES_{AC}(b,t) = ES_{AC}(b, t - 1) + (\eta_c P_{AC}^c(b,t)$$
$$- \eta_d P_{AC}^d(b,t))\Delta t,$$
$$\forall t \in T - \{1\}, \ \forall b \in S_{bus_{AC}} \quad (23)$$

Similar to AC subgrid, the constraints relating to DC subgrid can be found hereafter. The active power balance equation at each bus b are shown in (24) and (25). Equations (26), (27) and (28) represent the the operational constraints regarding voltage limits, line capacities and the power generation limit of conventional generators, while constraints (29)-(33) corresponds to the BESS unit in DC subgrid. More details about modeling a DC MG can be found in [37]. Considering the non-linear constraints (5)-(6) pertaining to the AC power flow formulation, a non-linear solver called 'IPOPT' is employed in this paper to solve the operational problem [40].

$$P_{DC}^d(b,t) - P_{DC}^c(b,t) + \sum_{g \in NG_b} P_{DC}(g,t)$$
$$+ P_{ls_{DC}}(b,t)$$
$$= P_{DC}^{ex}(b,t) + P_{l_{DC}}(b,t)$$
$$+ P_{os_{DC}}(b,t) - P_{ic}(t) \quad (24)$$

$$P_{DC}^{ex}(b,t) = \sum_{p \in N_{bus_{DC}}} V_{DC}(b,t)V_{DC}(p,t)G_{bp},$$
$$\forall t \in T, \ \forall b \in N_{bus_{DC}} \quad (25)$$

$$V_{DC}^{min} \le V_{DC}(b,t) \le V_{DC}^{max},$$
$$\forall t \in T, \ \forall b \in N_{bus_{DC}} \quad (26)$$

$$max(S_{DC}(i,t)) \le S_{DC}^{lim}(i),$$
$$\forall t \in T, \ \forall i \in N_{br_{DC}} \quad (27)$$

$$P_{g_{DC}}^{min} \le P_{DC}(g,t) \le P_{g_{DC}}^{max},$$
$$\forall t \in T, \ \forall g \in N_{g_{DC}} \quad (28)$$

$$0 \le P_{DC}^c(b,t) \le P_{b_{DC}}^{max},$$
$$\forall t \in T, \ \forall b \in S_{bus_{DC}} \quad (29)$$

$$0 \le P_{DC}^d(b,t) \le P_{b_{DC}}^{max},$$
$$\forall t \in T, \ \forall b \in S_{bus_{DC}} \quad (30)$$

$$P_{DC}^c(b,t) \cdot P_{DC}^d(b,t) = 0, \ \forall t \in T, \ \forall b \in S_{bus_{DC}} \quad (31)$$

$$ES_{b_{DC}}^{min} \le ES_{DC}(b,t) \le ES_{b_{DC}}^{max},$$
$$\forall t \in T, \forall b \in S_{bus_{DC}} \quad (32)$$

$$ES_{DC}(b,t) = ES_{DC}(b, t - 1) + (\eta_c P_{DC}^c(b,t)$$
$$- \eta_d P_{DC}^d(b,t))\Delta t,$$
$$\forall t \in T - \{1\}, \ \forall b \in S_{bus_{DC}} \quad (33)$$

B. EMERGENCY OPERATION MODE

In emergency mode, the objective is to minimize operational cost, given by (34), which due to the emergency situation would translate into maximization of load survivability. Note that load curtailment is coupled with a significantly high value of lost load c_{ls}.

$$F_2 = \sum_{t \in T_e} \sum_{g \in N_{g_{AC}}} c_g P_{AC}(g,t) + \sum_{t \in T_e} \sum_{b \in L_{bus_{AC}}} c_{ls} P_{ls_{AC}}(b,t)$$

$$+ \sum_{t \in T} \sum_{b \in S_{bus_{AC}}} c_S^d P_{AC}^d(b,t) \eta_d$$

$$- \sum_{t \in T} \sum_{b \in S_{bus_{AC}}} c_S^c P_{AC}^c(b,t) \eta_c$$

$$+ \sum_{t \in T_e} \sum_{b \in L_{bus_{AC}}} c_{os} P_{os_{AC}}(b,t)$$

$$+ \sum_{t \in T_e} \sum_{g \in N_{g_{DC}}} c_g P_{DC}(g,t) + \sum_{t \in T_e} \sum_{b \in L_{bus_{AC}}} c_{ls} P_{ls_{DC}}(b,t)$$

$$+ \sum_{t \in T} \sum_{b \in S_{bus_{DC}}} c_S^d P_{DC}^d(b,t) \eta_d$$

$$- \sum_{t \in T} \sum_{b \in S_{bus_{DC}}} c_S^c P_{DC}^c(b,t) \eta_c$$

$$+ \sum_{t \in T_e} \sum_{b \in L_{bus_{DC}}} c_{os} P_{os_{DC}}(g,t) \quad (34)$$

Except for equation (3), which is now modified into equation (35), the rest of constraints in this mode are the same as those in resilience operation mode. Furthermore, it is assumed that the MG has limited generation resources, which accounts for equations (36) and (37). Equations (38)-(40) correspond to the demand response in AC subgrid, where the ratio β_f ($0 \leq \beta_f \leq 1$) represents the maximum percentage of load type f for load shift and T_f is the allowed shifting horizon for load type f. $\beta_f = 0$ implies that load f does not exhibit any time-shifting flexibility, while $\beta_f = 1$ implies that the whole demand can be shifted in the given time horizon. Constraint (38) ensures that load shifting is energy neutral for any types of loads within the operating horizon and we assume that load shifting does not involve energy losses. In equation (39), $P_{l_{AC_{base}}}(b,t)$ means the total base load without load shifting and $P_{l_{AC}}(b,t)$ exhibits the total load of bus b at time point t after load shifting.

$$P_{AC}^d(b,t) - P_{AC}^c(b,t) + \sum_{g \in NG_b} P_{AC}(g,t) + P_{ls_{AC}}(b,t)$$

$$= P^{ex}(b,t) + P_{l_{AC}}(b,t)$$

$$+ P_{os_{AC}}(b,t) + P_{ic}(t) \quad (35)$$

$$GS_{AC}(g,t) = GS_{AC}(g,t-1) - P_{AC}(g,t)\Delta t,$$
$$\forall t \in T_e - \{1\}, \quad \forall g \in N_{g_{AC}} \quad (36)$$

$$GS_{g_{AC}}^{min} \leq GS_{AC}(b,t) \leq GS_{g_{AC}}^{ini},$$
$$\forall t \in T, \ \forall g \in N_{g_{AC}} \quad (37)$$

$$- \beta_f P_{l_{AC}}(b,f,t) \leq P_{lsh_{AC}}(b,f,t)$$
$$\leq \beta_f P_{l_{AC}}(b,f,t),$$
$$\forall t \in T_f, \quad \forall f \in N_{L_{AC}}, \forall b \in N_{bus_{AC}} \quad (38)$$

$$\sum_{t \in T_f} P_{lsh_{AC}}(b,f,t) = 0, \forall f \in N_{L_{AC}}, \forall b \in N_{bus_{AC}} \quad (39)$$

$$P_{l_{AC}}(b,t) = P_{l_{AC_{base}}}(b,t) + \sum_{f \in N_{L_{AC}}} P_{lsh_{AC}}(b,f,t),$$
$$\forall t \in T_f, \quad \forall b \in S_{bus_{AC}} \quad (40)$$

The above constraints related to limited generation resources and demand response in the AC subgrid also need to be duplicated and modified for the DC subgrid, which can be found hereafter. The limitation of generation resources accounts for equations (41) and (42), while equations (43)-(45) correspond to the demand response in DC subgrid.

$$GS_{DC}(g,t) = GS_{DC}(g,t-1) - P_{DC}(g,t)\Delta t,$$
$$\forall t \in T_e - \{1\}, \quad \forall g \in N_{g_{DC}} \quad (41)$$

$$GS_{g_{DC}}^{min} \leq GS_{DC}(b,t) \leq GS_{g_{DC}}^{ini}, \quad \forall t \in T, \ \forall g \in N_{g_{DC}} \quad (42)$$

$$- \beta_f P_{l_{DC}}(b,f,t) \leq P_{lsh_{DC}}(b,f,t)$$
$$\leq \beta_f P_{l_{DC}}(b,f,t),$$
$$\forall t \in T_f, \quad \forall f \in N_{L_{DC}},$$
$$\forall b \in N_{bus_{DC}} \quad (43)$$

$$\sum_{t \in T_f} P_{lsh_{DC}}(b,f,t) = 0, \quad \forall f \in N_{L_{DC}}, \ \forall b \in N_{bus_{DC}} \quad (44)$$

$$P_{l_{DC}}(b,t) = P_{l_{DC_{base}}}(b,t)$$
$$+ \sum_{f \in N_{L_{DC}}} P_{lsh_{DC}}(b,f,t),$$
$$\forall t \in T_f, \quad \forall b \in S_{bus_{DC}} \quad (45)$$

IV. CASE STUDIES

We assume that the first warning occurs at $t = 0$, and then the hybrid MG switches into resilience operation mode to import power from main grid and be prepared. When the extreme event occurs, the MG switches into islanded mode (the occurring time remains uncertain) to protect itself for at least two days. To appropriately present the advantages of BESS units on resilience enhancement, the day-ahead scheduling method is employed to run the AC OPF algorithm to make decisions about power output of generators, power exchange and battery energy management. WT and PV devices are considered as non-dispatchable generation resources and have a capacity of 100 kW and 50 kW respectively, while wind power, solar power and load profiles are extracted from [26] and can be found in Fig. 3. The parameters associated with lines, generators and BESSs are specified in Table. 1-3 respectively.

A. SIMULATION I - PREVENTIVE POWER IMPORTING

We assume there are 15000 kWh energy reserve in AC subgrid and 6000 kWh energy reserve in DC subgrid. Note that, according to this assumption, the AC subgrid has enough energy to support itself for a long period, while the DC subgrid has a large risk of energy deficiency. In the first investigated scenario, the hybrid MG needs to be prepared at every time point (from t = 0h to t = 11h) in the preventive stage. Note that a sensitivity analysis on different event occurrence time will be shown later to capture the uncertain nature of an extreme event. A 48-hour islanding period is considered as the emergency situation to appropriately present
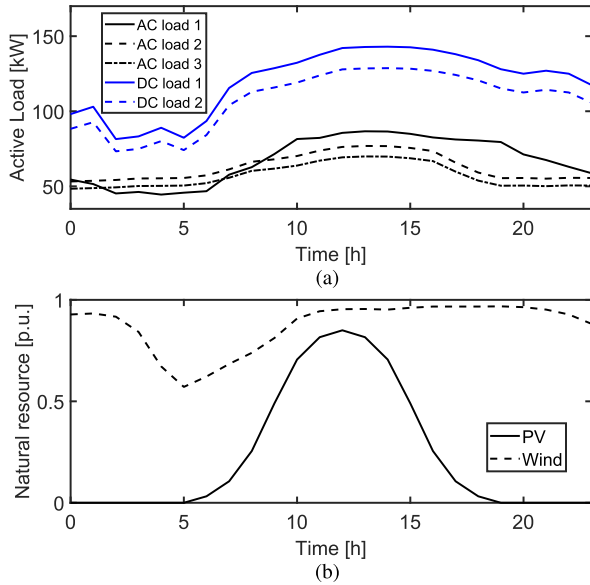
FIGURE 3. (a) Load profiles, (b) Wind profiles and PV profiles.

TABLE 1. Line data corresponding to the hybrid AC/DC MG of Figure 2.

Line between bus i → j	Reactance $(X_{li}[p.u.])$	Resistance $(R_{li}[p.u.])$	Capacitance $(C_{li}[p.u.])$	Maximum flow [MVA]
0 → 1	0.200	0.100	0.040	100
0 → 3	0.200	0.050	0.040	100
0 → 4	0.300	0.080	0.060	100
1 → 2	0.250	0.050	0.060	60
1 → 3	0.100	0.050	0.020	60
1 → 4	0.300	0.100	0.040	60
1 → 5	0.200	0.070	0.050	60
2 → 4	0.260	0.120	0.050	60
2 → 5	0.100	0.020	0.020	60
3 → 4	0.400	0.200	0.080	60
4 → 5	0.300	0.100	0.060	60
6 → 7	-	1.040	-	120
6 → 8	-	1.040	-	120

TABLE 2. Characteristics of generators in the hybrid MG.

Type	Subgrid	Min-Max Capacity (kW)
Diesel generator	AC subgrid	0-150
Fuel cell	DC subgrid	0-150

TABLE 3. Characteristics of BESS units in the hybrid MG.

Type	Subgrid	Min-Max SOC (kWh)	Power capacity (kW)	Initial SOC (kWh)
BESS	AC subgrid	0-200	50	100
BESS	DC subgrid	0-2000	100	100

the advantages of the proposed resilience strategy and the impacts of energy deficiency. Furthermore, a strategy which does not consider preventive power importing (i.e. base case without resilience enhancement) is simulated for comparison. The objective function of the base case ignores the last two terms in equation (2), which means that no preventive power importing strategy is applied. Constraints in the base case are the same as those in the resilience case.
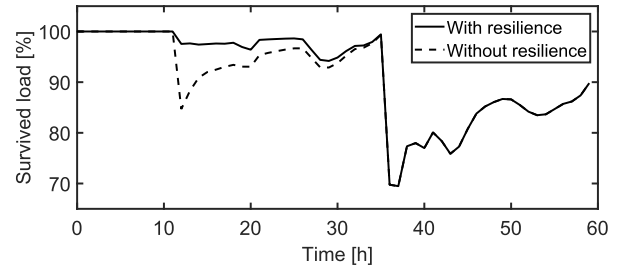

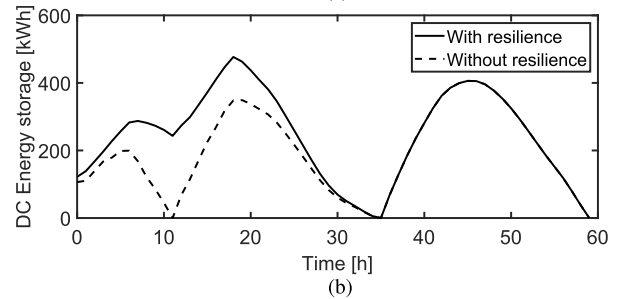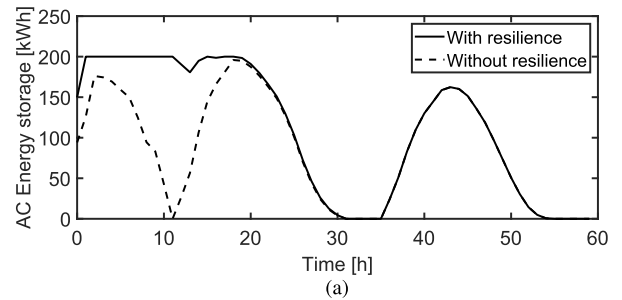**FIGURE 4.** Simulation I: Percentage of survived load.

FIGURE 5. Simulation I: (a) Battery storage change in AC subgrid, (b) Battery storage change in DC subgrid.

Fig. 4 shows that load shedding occurs in both cases when the hybrid MG switches into islanded mode, because of the interrupted connection between the MG and main grid. Additionally, the proposed resilience strategy results in less load shedding in the first 24-hour islanded period than the strategy without resilience. The reason is that more energy is stored in BESS units through power importing in preventive stage. Fig. 5(a)-5(b) indicate that storage units in both AC and DC sides charge in the preventive stage and keep a high state of energy. As one of the most common proactive ways to enhance resilience, the advantages of preventive power importing have been appropriately presented.

Fig. 5(b) exhibits that the battery slightly discharges in the last few hours of the preventive stage even though preventive power importing is applied. The reason is that the power flow through the line between bus 6→7 reaches its capacity in the last few hours (from t=6h to t=11h) of the preventive stage, which can be observed in Fig. 6(a). This means that no more power can be injected into bus 7 through the line between bus 6→7 and the battery shall discharge to avoid load shedding when the load level in bus 7 increases. Additionally, the power through line 6→7 exhibits a drop from t=2h to t=5h. The reason can be found in Fig. 6(b), which indicates the voltage
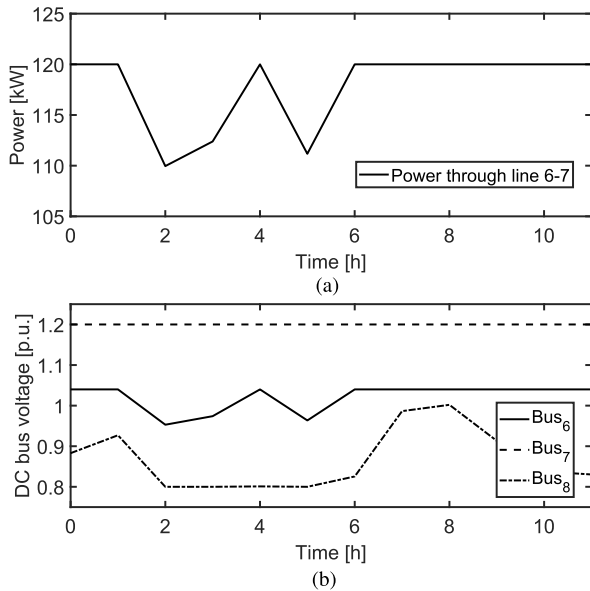
FIGURE 6. Simulation I: (a) Power flow through the line between bus 6→7 at the preventive stage (with resilience), (b) Bus voltage in DC subgrid at the preventive stage (with resilience).

TABLE 4. Resilience index in Simulation I.

	No resilience	With resilience
RI (12-59h)	0.1166	0.1020
RI (12-35h)	0.0566	0.0273
RI (36-59h)	0.1766	0.1766

FIGURE 7. Simulation I: Sensitivity analysis on different event occurrence time points.

profiles in all DC buses during the preventive stage. Note that both DC load 1 and DC load 2 have the lowest level from t=2h to t=5h, meaning that the voltage in bus 8 shall drop to ensure power balance and to satisfy the detailed power flow equations utilized in this OPF algorithm. Fig. Fig. 6(b) shows that the voltage level in bus 8 has reached its minimum from t=2h to t=5h. As such, to match the low load level in bus 8, the voltage in bus 6 shall drop to reduce the power flow through line 6→8. It can be observed that the voltage level in bus 7 reaches its maximum and remains constant, which means the drop of the voltage level in bus 6 also reduces the power flow through line 6→7. It can be concluded that the power flow drop from t=2h to t=5h is a result of the constraints relating to voltage, which strongly supports the utilization of a detailed AC OPF towards capturing more realistic results.

However, in the second 24-hour period, both cases yield large load shedding, because of the deficiency of generation resources in DC subgrid. Fig. 4 also illustrates that the proposed strategy only has a positive effect on load survivability in the first 24 hours of islanded mode. The reason is that imported power in the proposed strategy is not enough to support a longer islanding period, because of the limitation of battery capacity and the duration of preventive stage. The further load shedding primarily demonstrates the impact of energy deficiency on resilience and supports the introduction of the proposed multi-phase resilience curve, as a method to capture it appropriately.

With respect to the suggested resilience index, Table. 4 shows that, the proposed strategy obtains a smaller *RI* value (0.0273) in the first 24 hours than the strategy without resilience (0.0566), while the same *RI* value is achieved in both cases during the last 24 hours because of the energy

deficiency in DC subgrid. Note that this case doesn't consider the discrimination of loads into critical and non-critical and the values of w_c and w_n are same. To summarize, with the consideration of preventive power importing, the resilience of the AC/DC hybrid MG (*RI* value from 0.1166 to 0.1020) is enhanced.

Note that we also assume that the event may happen at any time point in the preventive stage because of its uncertain nature. In this scenario, the hybrid MG needs to be prepared at every time point from receiving the first warning about an event to event occurrence. To entirely present the effects of preventive power importing on resilience enhancement, a sensitivity analysis on different event occurrence time is done and the results can be seen as follows. Fig. 7 shows that the case with resilience obtained less load shedding than the case without resilience for all the different time points of event occurrence. It can also be concluded that a longer preventive stage allows more power injection and achieves more resilience.

Another sensitivity analysis is done for the influence of coefficients α_{AC} and α_{DC} on the amount of total injected energy, which accounts for the BESSs in both AC subgrid and DC subgrid. Fig. 8 shows that more energy is injected when the values of coefficients increase, compared with the power exchange price C_{ex}. Note that, after the values of coefficients are 1.2 times larger than C_{ex}, the amount of injected energy has reached the maximum and cannot be further increased.

B. SIMULATION II - DISCRIMINATION OF CRITICAL AND NON-CRITICAL LOADS

It is more realistic to assume that not all loads would be critical, hence this simulation extends the model by introducing discrimination of loads into critical and non-critical. For example, in a building-scale MG the critical loads could be lights and lift motors and the non-critical loads could be kitchen and toilet appliances [26]. Similar to [20], it is assumed that loads L_3 in bus 3 of AC subgrid (around 30%
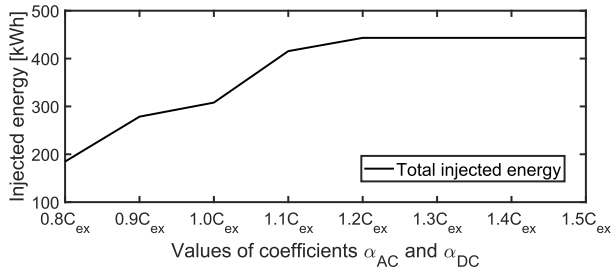
FIGURE 8. Simulation I: Sensitivity analysis on the values of coefficients α_{AC} and α_{DC}.

TABLE 5. Resilience index in Simulation II.

	No resilience	With resilience
RI (12-59h)	0.1184	0.1028
RI (12-35h)	0.0427	0.0117
RI (36-59h)	0.1940	0.1940

of total load) and L_7 in bus 7 of DC subgrid (around 50% of total load) are critical loads with high curtailment cost (w_c), while the rest of the loads are non-critical loads with relatively low curtailment cost (w_n). The proposed resilience strategy is employed to reduce load shedding and the base case without resilience is utilized for comparison purposes.

Similar to Simulation I, Fig. 9(b) shows that the resilience strategy achieves less load shedding in the first 24 hours than the base case without resilience and the further performance degradation in the last 24 hours verifies the accuracy of the proposed multi-phase resilience curve. Table. 5 illustrates that, with the consideration of critical loads and non-critical loads, the proposed resilience strategy still obtains a lower *RI* (0.1028) than the strategy without resilience (0.1184). The effect of preventive power importing on resilience is verified again.

Fig. 9(a) shows that the resilience strategy guarantees the survivability of critical loads in the first 24-hour islanding period, while the strategy without resilience causes 144.58 kWh load shedding of critical loads. Additionally, load shedding of non-critical loads is reduced from 422.43 kW to 273.82 kW. Note that, with the consideration of critical loads and non-critical loads, both cases obtain slightly larger total load shedding (273.82 kWh and 567.01 kWh) than the two cases in simulation I (272 kWh and 563.5 kWh), which means that more non-critical loads may be curtailed for the protection of critical loads.

Fig. 9(a) shows that, in the second 24-hour islanding period, both cases have a great deal of critical load shedding in DC subgrid. Note that the critical load shedding takes approximately 50% of total load shedding in the last 24 hours and all curtailed loads are from DC subgrid. In other words, the discrimination of critical and non-critical loads has no significant effects on reducing critical load shedding in the last 24 hours. A potential explanation to this would be the fact that DC voltage in bus 8 (connecting non-critical loads) is reaching its minimum allowed value (i.e. 0.8 p.u.) avoiding more
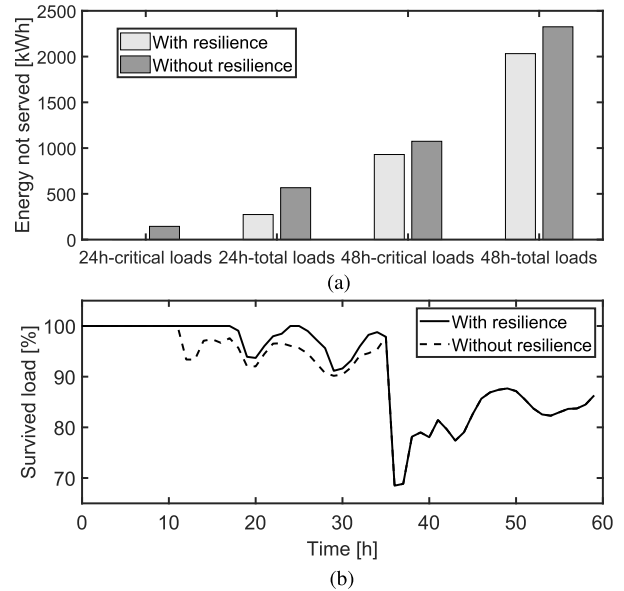

FIGURE 9. Simulation II: (a) Energy not served [kWh], (b) Percentage of survived load.

non-critical loads in bus 8 to be curtailed; this is illustrated in Fig. 10. Because of the voltage constraints, the hybrid MG has to curtail critical loads to ensure power balance. Note that voltage at bus 6 connected with a conventional generator is also down to the minimum value, which means no more loads can be supplied in this period. This is an important aspect of the proposed model, as typical energy management systems found in the literature would neglect the influence of voltage and obtain less critical load shedding; this would lead to violation of technical requirements. Even though more load shedding is caused through the proposed AC OPF algorithm, the result ensures an intact power system with no violation of technical requirements; this would be increasingly important in larger-scale MGs, as more and more MGs are embedded into distribution networks.

C. SIMULATION III - IMPACT OF DEMAND SHIFTING
Demand shifting may be one of the most effective and economic ways to reduce load shedding during extreme events, compared with other strategies (such as mobile energy resources (MERs) and electrical vehicles (EVs)). In this subsection, the effects of demand shifting on reducing load shedding and enhancing resilience are appropriately investigated. Preventive power importing and discrimination of loads into critical and non-critical are also considered. Note that the effect of limited generation resources has already been illustrated in simulations I and II, so a 24-hour islanding period is considered to simplify this case. Additionally, we assume that shiftable loads can be shifted across the whole scheduling horizon.

Fig. 11(a) shows that non-critical load shedding is gradually reduced as the percentage of shiftable loads increases; for clarity, no critical load shedding is caused when demand shifting is applied. However, when the percentage of shiftable
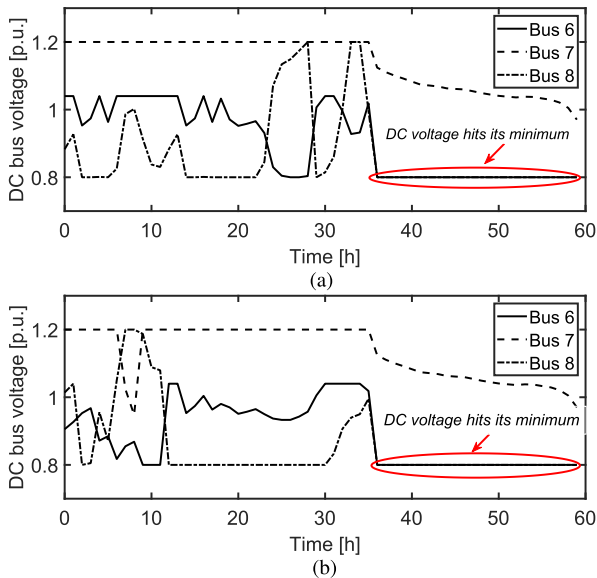
FIGURE 10. Simulation II: (a) Bus voltage in DC subgrid with resilience, (b) Bus voltage in DC subgrid without resilience.
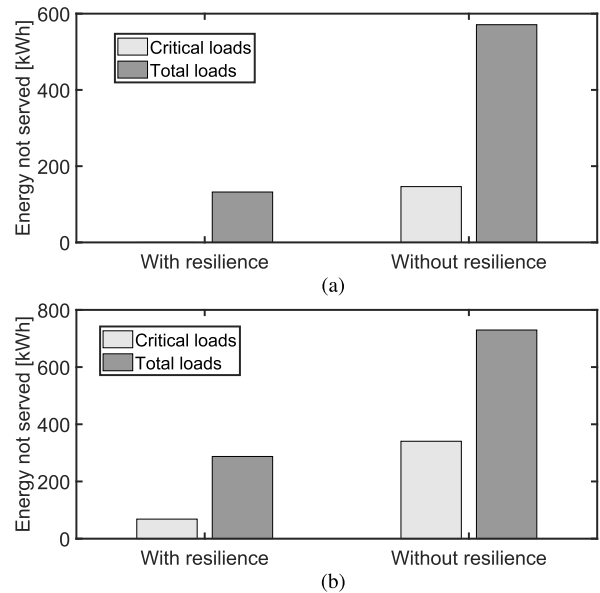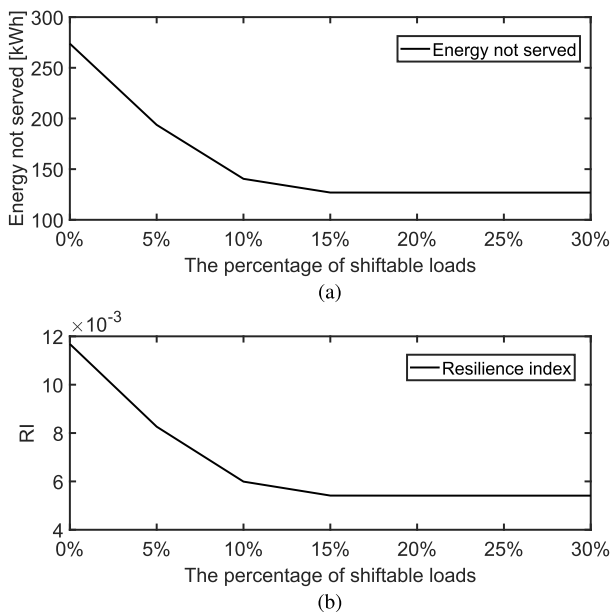

FIGURE 11. Simulation III: (a) Energy not served [kWh] for non-critical loads under different percentage of shiftable loads, (b) Change of RI with the percentage of shiftable loads.

loads is over 15%, demand shifting has no effects on load survivability. Fig. 11(b) shows the change of resilience index *RI*, which is reduced with the increase of the percentage of shiftable loads. When the percentage of shiftable loads is over 15%, resilience index *RI* reaches the minimum value (0.0054).

D. SIMULATION IV - IMPACT OF CONTINGENCIES

Most existing literature assumes that the structure of an islanded MG is intact during extreme events. However, a MG

FIGURE 12. Simulation IV: (a) Energy not served [kWh] under multiple line faults, (b) Energy not served [kWh] under interrupted connection.

can be damaged because of the highly uncertain nature of extreme events. To account for such cases, two types of contingencies including multiple line faults (contingency 1) and interrupted connection between AC and DC subgrids (contingency 2) are considered here to appropriately mimic a realistic scenario and further highlight the advantages of the proposed resilience strategy. Both preventive power importing and demand shifting (15% shiftable loads) are considered. As far as multiple line faults are concerned, it is assumed that the line between bus 3 and bus 4 and the line between bus 4 and bus 5 are damaged during the investigated event. Fig. 12 presents that the resilience strategy still obtains less load shedding than a strategy without resilience, while also the proposed strategy successfully protects critical loads in the first 24 hours after extreme events. Tab. 6 shows that the resilience strategy also obtains a lower resilience index *RI* (0.0056) than a strategy without resilience (0.0431).

In the simulated case, the power transfer from the AC subgrid to the DC subgrid supports the latter to reduce its load shedding. However, this connection can be interrupted during extreme events, as is the case in this simulation. Specifically, an interruption between the two subgrids has been modelled for 10 hours. Fig. 12(b) demonstrates that the proposed resilience strategy obtains much less critical load shedding (from 340.62 kWh to 68.37 kWh) and total load shedding (from 729.64 kWh to 336.09 kWh) than a strategy without resilience in the first 24 hour islanding period. Bus voltage changes in both cases are shown in Fig. 13. When the connection between the AC and DC subgrids is interrupted, DC voltages in all three buses are reduced and particularly bus 6 and bus 8 are down to the minimum value; see red circles on Fig. 13 indicating DC voltage reaching its minimum limit.
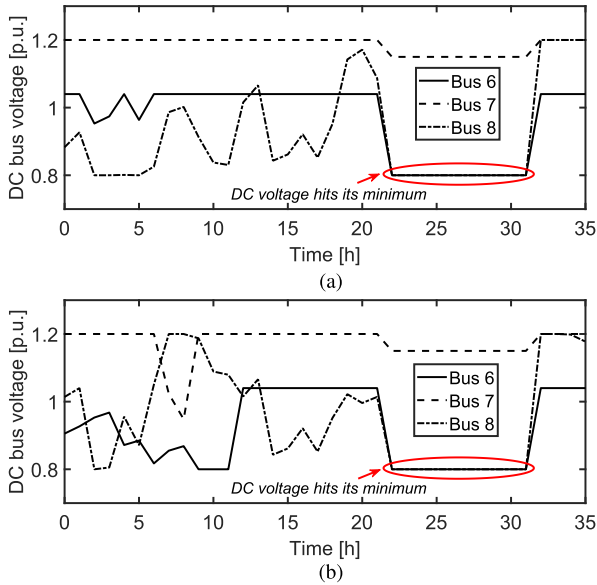
FIGURE 13. Simulation IV: (a) Bus voltage in DC subgrid under interrupted connection [with resilience], (b) Bus voltage in DC subgrid under interrupted connection [without resilience].

TABLE 6. Resilience index in Simulation IV.

	No resilience	With resilience
24h-RI (line faults)	0.0431	0.0056
24h-RI (interrupted connection)	0.0747	0.0210

TABLE 7. Comparison of costs between simulations II-IV.

	Preventive cost (£)	Generation cost (£)	Shedding cost (£)	Total cost (£)
S2 - Base case (without resilience)	423.16	943.18	50037.5	51403.84
S2 - Resilience case (no load shifting)	496.43	921.40	13691.40	15109.23
S3 - Resilience (5% shiftable loads)	496.43	933.42	9684.80	11114.65
S3 - Resilience (10% shiftable loads)	496.43	941.50	7022.10	8190.03
S3 - Resilience (15% shiftable loads)	496.43	943.52	6345.23	7785.18
S4 - Resilience and contingency 1	496.43	943.52	6609.67	8049.62

TABLE 8. Computational performance in Simulations II-IV.

	Solver time (s)	Solver status
S2 - Base case (without resilience)	146.72	Optimal
S2 - Resilience case (no load shifting)	81.65	Optimal
S3 - Resilience (5% shiftable loads)	125.45	Optimal
S3 - Resilience (10% shiftable loads)	152.15	Optimal
S3 - Resilience (15% shiftable loads)	144.44	Optimal
S4 - Resilience and contingency 1	190.20	Optimal

Table. 6 shows that the resilience strategy also obtains a lower resilience index *RI* (0.0210) than a strategy without resilience (0.0747). Even with the consideration of contingencies, the advantages of the proposed strategy are clearly shown with these results.

V. DISCUSSION

In Section IV, extensive simulations considering different case studies have been presented to verify the effectiveness of the proposed resilience strategy. In all simulations, the proposed resilience strategy obtains better solutions (lower load shedding and a better *RI* value) than a strategy without resilience. In simulations II-IV, the proposed resilience strategy successfully guarantees the survivability of critical loads in the first 24-hour period of the scheduling horizon. Table. 7 shows that, even though power importing brings slightly higher operation cost in preventive stage, it is worth employing this strategy for resilience purposes, as load survivability is more important than economical profits during emergency situations; of course this is appropriately reflected in the total operation cost. It can be deducted that the proposed strategy would become more economical if the event occurrence time is accurately predicted, because it only needs to improve the storage level of BESSs in one specific time point rather than the whole preventive stage. Table. 7 also shows that demand shifting is an effective way to balance load and power and reduce load shedding. With the increase of the percentage of

shiftable loads, the total operational cost is gradually reduced and the generation cost of conventional generators is slightly increased, which means that the energy has been more efficiently used for load survivability. Generally, the cost analysis presented in Table. 7 is consistent with the results for resilience index shown in previous sections. Table. 8 corresponds to the computational performance including solver time and solver status, where the mean computation time is 140.10 sec. All the simulations were run on Intel i7-8700u processor using 8 GB RAM.

In simulation II, it is hard to keep voltages within the imposed operational bounds because of the large resource deficiency in DC subgrid. When the voltage level in bus 8 reaches the minimum and no more non-critical loads can be curtailed, large critical load shedding is caused in the last 24 hours; see red circles in Fig. 10 indicating DC voltage reaching its minimum limit. Because of the existence of operational constraints, the suggested AC OPF algorithm obtained more accurate solutions (without violation of technical requirements) than EMS-based models. As far as the influence of limited generation resources is concerned, Fig. 14 shows that when the energy reserve in DC subgrid is increased, less load shedding is caused in the last 24 hours, while the ratio of critical load shedding and total load shedding is reduced meaning that large energy deficiency can cause additional critical load shedding.

In simulation IV, when the connection between the AC and DC subgrids is interrupted for 10 hours, critical load
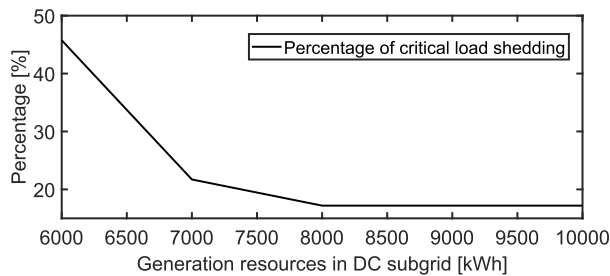
FIGURE 14. Influence of limited generation resources on critical load shedding in the last 24 hours.

shedding is caused (68.37 kWh) in the DC subgrid in the first 24 hours, even though preventive power importing and demand shifting are employed to balance generation and load. This indicates that it may not be enough for a MG to only employ operational strategies to guarantee critical load survivability when extreme events occur. Developing appropriate planning strategies (e.g. to account for optimal sizing of battery units and generators) or infrastructure-oriented strategies (e.g. line hardening and dispatch of repair crews) is important.

VI. CONCLUSION

In this paper, a resilience strategy based on preventive power importing and demand response is proposed to enhance the resilience of AC/DC hybrid MGs during extreme events. Both grid-connected and islanded modes are considered in the presented model. Preventive power importing is used to prepare the MG for future events, while demand response is employed to reduce load shedding and operational cost during emergency mode. A detailed OPF algorithm considering operational constraints is adopted to formulate the non-linear problem. In addition, a modified multi-phase resilience curve and consequently an area resilience index are suggested to fully exhibit the influence of limited generation resources and uncertain event duration on resilience assessment. Extensive simulations are conducted to show the advantages of the proposed resilience strategy on reducing load shedding, guaranteeing critical load survivability and reducing operational cost, while proving the necessity for the modified multi-phase resilience curve. An effective sensitivity analysis on different event occurrence time has been simulated to capture the uncertain nature of extreme events. The impact of limited generation resources, the discrimination of loads into critical and non-critical, demand shifting and contingencies on load survivability are appropriately illustrated.

Future work can focus on developing a stochastic model or utilizing robust optimization to capture the main uncertainties surrounding extreme events. Furthermore, dynamic control of hybrid AC/DC MGs relating to frequency and voltage is important in the area of power system analysis, especially for resilience-driven problems. Effective dynamic models needs to be developed to ensure that a frequency and voltage-representative scenario is captured.

REFERENCES

[1] M. Panteli, P. Mancarella, D. N. Trakas, E. Kyriakides, and N. D. Hatziargyriou, "Metrics and quantification of operational and infrastructure resilience in power systems," *IEEE Trans. Power Syst.*, vol. 32, no. 6, pp. 4732–4742, Nov. 2017.

[2] M. Panteli and P. Mancarella, "The grid: Stronger, bigger, smarter?: Presenting a conceptual framework of power system resilience," *IEEE Power Energy Mag.*, vol. 13, no. 3, pp. 58–66, May 2015.

[3] G. Strbac, N. Hatziargyriou, J. P. Lopes, C. Moreira, A. Dimeas, and D. Papadaskalopoulos, "Microgrids: Enhancing the resilience of the European megagrid," *IEEE Power Energy Mag.*, vol. 13, no. 3, pp. 35–43, May 2015.

[4] A. Khodaei, "Microgrid optimal scheduling with multi-period islanding constraints," *IEEE Trans. Power Syst.*, vol. 29, no. 3, pp. 1383–1392, May 2014.

[5] A. Khodaei, "Resiliency-oriented microgrid optimal scheduling," *IEEE Trans. Smart Grid*, vol. 5, no. 4, pp. 1584–1591, Jul. 2014.

[6] A. Gholami, T. Shekari, F. Aminifar, and M. Shahidehpour, "Microgrid scheduling with uncertainty: The quest for resilience," *IEEE Trans. Smart Grid*, vol. 7, no. 6, pp. 2849–2858, Nov. 2016.

[7] A. Gholami, T. Shekari, and S. Grijalva, "Proactive management of microgrids for resiliency enhancement: An adaptive robust approach," *IEEE Trans. Sustain. Energy*, vol. 10, no. 1, pp. 470–480, Jan. 2019.

[8] M. Tavakoli, F. Shokridehaki, M. Funsho Akorede, M. Marzband, I. Vechiu, and E. Pouresmaeil, "CVaR-based energy management scheme for optimal resilience and operational cost in commercial building microgrids," *Int. J. Electr. Power Energy Syst.*, vol. 100, pp. 1–9, Sep. 2018.

[9] E. Rosales-Asensio, M. de Simón-Martín, D. Borge-Diez, J. J. Blanes-Peiró, and A. Colmenar-Santos, "Microgrids with energy storage systems as a means to increase power resilience: An application to office buildings," *Energy*, vol. 172, pp. 1005–1015, Apr. 2019.

[10] H. Lee, G.-S. Byeon, J.-H. Jeon, A. Hussain, H.-M. Kim, A. O. Rousis, and G. Strbac, "An energy management system with optimum reserve power procurement function for microgrid resilience improvement," *IEEE Access*, vol. 7, pp. 42577–42585, 2019.

[11] M. H. Amirioun, F. Aminifar, and H. Lesani, "Towards proactive scheduling of microgrids against extreme floods," *IEEE Trans. Smart Grid*, vol. 9, no. 4, pp. 3900–3902, Jul. 2018.

[12] M. H. Amirioun, F. Aminifar, and H. Lesani, "Resilience-oriented proactive management of microgrids against windstorms," *IEEE Trans. Power Syst.*, vol. 33, no. 4, pp. 4275–4284, Jul. 2018.

[13] S. D. Manshadi and M. E. Khodayar, "Resilient operation of multiple energy carrier microgrids," *IEEE Trans. Smart Grid*, vol. 6, no. 5, pp. 2283–2292, Sep. 2015.

[14] H. Lei, S. Huang, Y. Liu, and T. Zhang, "Robust optimization for microgrid defense resource planning and allocation against multi-period attacks," *IEEE Trans. Smart Grid*, vol. 10, no. 5, pp. 5841–5850, Sep. 2019.

[15] H. Gao, Y. Xu, C.-C. Liu, and Y. Chen, "Dynamic load shedding for an islanded microgrid with limited generation resources," *IET Gener., Transmiss. Distrib.*, vol. 10, no. 12, pp. 2953–2961, Sep. 2016.

[16] K. Balasubramaniam, P. Saraf, R. Hadidi, and E. B. Makram, "Energy management system for enhanced resiliency of microgrids during islanded operation," *Electr. Power Syst. Res.*, vol. 137, pp. 133–141, Aug. 2016.

[17] M. Chen, X. Xiao, and J. M. Guerrero, "Secondary restoration control of islanded microgrids with a decentralized event-triggered strategy," *IEEE Trans. Ind. Informat.*, vol. 14, no. 9, pp. 3870–3880, Sep. 2018.

[18] M. Hosseinzadeh and F. R. Salmasi, "Power management of an isolated hybrid AC/DC micro-grid with fuzzy control of battery banks," *IET Renew. Power Gener.*, vol. 9, no. 5, pp. 484–493, Jul. 2015.

[19] M. S. Mahmoud, F. M. A. L.-Sunni, and M. S. Ur Rahman, "Review of microgrid architectures—A system of systems perspective," *IET Renew. Power Gener.*, vol. 9, no. 8, pp. 1064–1078, Nov. 2015.

[20] A. Hussain, V.-H. Bui, and H.-M. Kim, "Optimal operation of hybrid microgrids for enhancing resiliency considering feasible islanding and survivability," *IET Renew. Power Gener.*, vol. 11, no. 6, pp. 846–857, May 2017.

[21] A. Hussain, V.-H. Bui, and H.-M. Kim, "Fuzzy logic-based operation of battery energy storage systems (BESSs) for enhancing the resiliency of hybrid microgrids," *Energies*, vol. 10, no. 3, p. 271, Feb. 2017.

[22] A. Hussain, V.-H. Bui, and H.-M. Kim, "A proactive and survivability-constrained operation strategy for enhancing resilience of microgrids using energy storage system," *IEEE Access*, vol. 6, pp. 75495–75507, 2018.

[23] A. Hussain, A. Oulis Rousis, I. Konstantelos, G. Strbac, J. Jeon, and H.-M. Kim, "Impact of uncertainties on resilient operation of microgrids: A data-driven approach," *IEEE Access*, vol. 7, pp. 14924–14937, 2019.

[24] H. Qiu, W. Gu, Z. Wu, S. Zhou, G. Pan, X. Yang, X. Yuan, and X. Ding, "Resilience-directional robust power dispatching of microgrids under meteorological disasters," *IET Renew. Power Gener.*, vol. 13, no. 12, pp. 2084–2093, Sep. 2019.

[25] J. Liu, X. Lu, and J. Wang, "Resilience analysis of DC microgrids under denial of service threats," *IEEE Trans. Power Syst.*, vol. 34, no. 4, pp. 3199–3208, Jul. 2019.

[26] A. O. Rousis, I. Konstantelos, and G. Strbac, "A planning model for a hybrid AC–DC microgrid using a novel GA/AC OPF algorithm," *IEEE Trans. Power Syst.*, vol. 35, no. 1, pp. 227–237, Jan. 2020.

[27] K. P. Schneider, N. Radhakrishnan, Y. Tang, F. K. Tuffner, C.-C. Liu, J. Xie, and D. Ton, "Improving primary frequency response to support networked microgrid operations," *IEEE Trans. Power Syst.*, vol. 34, no. 1, pp. 659–667, Jan. 2019.

[28] M. Panteli, D. N. Trakas, P. Mancarella, and N. D. Hatziargyriou, "Power systems resilience assessment: Hardening and smart operational enhancement strategies," *Proc. IEEE*, vol. 105, no. 7, pp. 1202–1213, Jul. 2017.

[29] M. H. Amirioun, F. Aminifar, H. Lesani, and M. Shahidehpour, "Metrics and quantitative framework for assessing microgrid resilience against windstorms," *Int. J. Electr. Power Energy Syst.*, vol. 104, pp. 716–723, Jan. 2019.

[30] M. H. Amirioun, F. Aminifar, and M. Shahidehpour, "Resilience-promoting proactive scheduling against hurricanes in multiple energy carrier microgrids," *IEEE Trans. Power Syst.*, vol. 34, no. 3, pp. 2160–2168, May 2019.

[31] H. Gao, Y. Chen, Y. Xu, and C.-C. Liu, "Resilience-oriented critical load restoration using microgrids in distribution systems," *IEEE Trans. Smart Grid*, vol. 7, no. 6, pp. 2837–2848, Nov. 2016.

[32] S. Yao, P. Wang, and T. Zhao, "Transportable energy storage for more resilient distribution systems with multiple microgrids," *IEEE Trans. Smart Grid*, vol. 10, no. 3, pp. 3331–3341, May 2019.

[33] Z. Li, M. Shahidehpour, F. Aminifar, A. Alabdulwahab, and Y. Al-Turki, "Networked microgrids for enhancing the power system resilience," *Proc. IEEE*, vol. 105, no. 7, pp. 1289–1310, Jul. 2017.

[34] S. Mousavizadeh, M.-R. Haghifam, and M.-H. Shariatkhah, "A linear two-stage method for resiliency analysis in distribution systems considering renewable energy and demand response resources," *Appl. Energy*, vol. 211, pp. 443–460, Feb. 2018.

[35] J. Najafi, A. Peiravi, and J. M. Guerrero, "Power distribution system improvement planning under hurricanes based on a new resilience index," *Sustain Cities Soc.*, vol. 39, pp. 592–604, May 2018.

[36] X. Liu, M. Shahidehpour, Z. Li, X. Liu, Y. Cao, and Z. Bie, "Microgrids for enhancing the power grid resilience in extreme conditions," *IEEE Trans. Smart Grid*, vol. 8, no. 2, pp. 589–597, Mar. 2017.

[37] A. A. Eajal, M. A. Abdelwahed, E. F. El-Saadany, and K. Ponnambalam, "A unified approach to the power flow analysis of AC/DC hybrid microgrids," *IEEE Trans. Sustain. Energy*, vol. 7, no. 3, pp. 1145–1158, Jul. 2016.

[38] Y. Xia, W. Wei, M. Yu, X. Wang, and Y. Peng, "Power management for a hybrid AC/DC microgrid with multiple subgrids," *IEEE Trans. Power Electron.*, vol. 33, no. 4, pp. 3520–3533, Apr. 2018.

[39] Y. Xia, Y. Peng, P. Yang, M. Yu, and W. Wei, "Distributed coordination control for multiple bidirectional power converters in a hybrid AC/DC microgrid," *IEEE Trans. Power Electron.*, vol. 32, no. 6, pp. 4949–4959, Jun. 2017.

[40] A. Wächter and L. T. Biegler, "On the implementation of an interior-point filter line-search algorithm for large-scale nonlinear programming," *Math. Program.*, vol. 106, no. 1, pp. 25–57, Mar. 2006.

YI WANG (Student Member, IEEE) is currently pursuing the Ph.D. degree with Imperial College London. His research interests include mathematical programming applied to the planning and operation of distribution systems, while he focuses on the resilience enhancement of the future power systems.

ANASTASIOS OULIS ROUSIS (Member, IEEE) is currently a Research Associate with Imperial College London. His expertise in power system optimization and renewable integration. His current work involves optimization of planning and operational models for transmission and distribution systems, including microgrids, while he investigates how flexible technologies can enhance the development of the future power systems.

GORAN STRBAC (Member, IEEE) is currently a Professor of energy systems with Imperial College London, London, U.K. His current research interests include modeling and optimization of economics, security of energy system operation and investment, energy infrastructure reliability, and future energy markets, including integration of emerging technologies in supporting cost-effective evolution to smart low-carbon energy future.

• • •